## Article

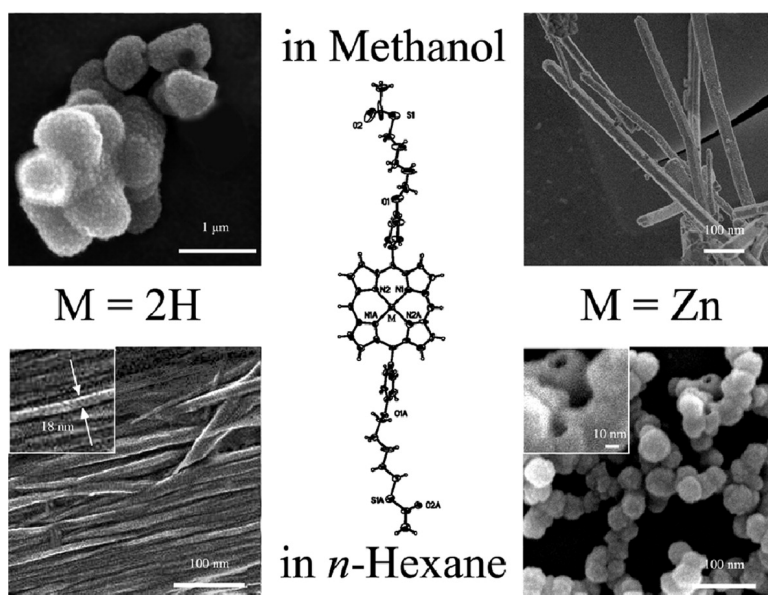# Morphology-Controlled Self-Assembled Nanostructures of 5,15-Di[4-(5-acetylsulfanylpentyloxy)phenyl]porphyrin Derivatives. Effect of Metal#Ligand Coordination Bonding on Tuning the Intermolecular Interaction

Yingning Gao, Xiaomei Zhang, Changqin Ma, Xiyou Li, and Jianzhuang Jiang

## More About This Article

Additional resources and features associated with this article are available within the HTML version:

- Supporting Information
- Access to high resolution figures
- Links to articles and content related to this article
- Copyright permission to reproduce figures and/or text from this article

**View the Full Text HTML**

# J|A|C|S

## A R T I C L E S

# Morphology-Controlled Self-Assembled Nanostructures of 5,15-Di[4-(5-acetylsulfanylpentyloxy)phenyl]porphyrin Derivatives. Effect of Metal–Ligand Coordination Bonding on Tuning the Intermolecular Interaction

Yingning Gao, Xiaomei Zhang, Changqin Ma, Xiyou Li, and Jianzhuang Jiang*

*Department of Chemistry, Shandong University, Jinan 250100, China*

Received August 26, 2008; E-mail: jzjiang@sdu.edu.cn

***Abstract:*** Novel metal-free 5,15-di[4-(5-acetylsulfanylpentyloxy)phenyl]porphyrin $H_2[DP(CH_3COSC_5H_{10}O)_2P]$ (**1**) and its zinc congener $Zn[DP(CH_3COSC_5H_{10}O)_2P]$ (**2**) were designed and synthesized. Single-crystal X-ray diffraction (XRD) analysis confirmed the tetrapyrrole nature of these two compounds, revealing the existence of metal–ligand coordination bond between the carbonyl oxygen in the aryloxy side chain of meso-attached phenyl group in the porphyrin molecule with the zinc center of neighboring porphyrin molecule in the crystal structure of **2**. This intermolecular Zn–O coordination bond induces the formation of a supramolecular chain structure in which the porphyrinato zinc moieties are arranged in a "head-to-tail" mode (*J*-aggregate), which is in contrast to a "face-to-face" stacking mode (*H*-aggregate) in the supramolecular structure formed depending on the C–H···$\pi$ interaction in the crystal of **1**. Their self-assembling properties in MeOH and *n*-hexane were comparatively investigated by scanning electronic microscopy and XRD technique. Intermolecular $\pi$–$\pi$ interaction of metal-free porphyrin **1** leads to the formation of hollow nanospheres and nanoribbons in MeOH and *n*-hexane, respectively. In contrast, introduction of additional Zn–O coordination bond for porphyrinato zinc complex **2** induces competition with intermolecular $\pi$–$\pi$ interaction, resulting in nanostructures with nanorod and hollow nanosphere morphology in MeOH and *n*-hexane. The IR and XRD results clearly reveal the presence and absence of such metal–ligand coordination bond in the nanostructures formed from porphyrinato zinc complex **2** and metal-free porphyrin **1**, respectively, which is further unambiguously confirmed by the single-crystal XRD analysis result for both compounds. Electronic absorption spectroscopic data on the self-assembled nanostructures reveal the *H*-aggregate nature in the hollow nanospheres and nanoribbons formed from metal-free porphyrin **1** due to the $\pi$–$\pi$ intermolecular interaction between porphyrin molecules and *J*-aggregate nature in the nanorods and hollow nanospheres of **2** depending on the dominant metal–ligand coordination bonding interaction among the porphyrinato zinc molecules. The present result appears to represent the first effort toward controlling and tuning the morphology of self-assembled nanostructures of porphyrin derivatives via molecular design and synthesis through introduction of metal–ligand coordination bonding interaction. Nevertheless, availability of single crystal and molecular structure revealed by XRD analysis for both porphyrin derivatives renders it possible to investigate the formation mechanism as well as the molecular packing conformation of self-assembled nanostructures of these typical organic building blocks with large conjugated system in a more confirmed manner.

## Introduction

Self-assembled nanostructures have created a wide range of ever more sophisticated molecular materials associated with their diverse applications. In particular, self-assembly of functional molecular materials with large conjugated electronic structure into well-defined nanostructures depending on various noncovalent interactions has attracted increasing research interests in both material and chemistry fields.[1–8] On the basis of different noncovalent intermolecular interactions, a wide variety of nanostructures such as particles, fibers, rods, sheets, cubes, and tubes have been fabricated with potential application in the fields of sensors,[9–12] field-effect transistors,[13–15] and photovoltaics.[16–21]

Extensive investigations have revealed that self-assembly of conjugated molecular systems depends mainly on the intermolecular $\pi$–$\pi$ interaction. Introduction of different functional

groups onto the peripheral positions of conjugated molecules with rigid molecular structure induces additional intermolecular interactions including van der Waals, hydrogen bonding, hydrophilic/hydrophobic, electrostatic, and metal–ligand coordina-

(1) Hill, D. J.; Mio, M. J.; Prince, R. B.; Hughes, T. S.; Moore, J. S. *Chem. Rev.* **2001**, *101*, 3893–4012.

(2) Lehn, J.-M. *Supramolecular Chemistry*; Verlag Chimie: Weinheim, Germany, 1995.

(3) Elemans, J. A. A. W.; van Hameren, R.; Nolte, R. J. M.; Rowan, A. E. *Adv. Mater.* **2006**, *18*, 1251–1226.

(4) (a) Hartgerink, J. D.; Beniash, E.; Stupp, S. I. *Science* **2001**, *294*, 1684–1688. (b) Kitamura, T.; Nakaso, S.; Mizoshita, N.; Tochigi, Y.; Shimomura, T.; Moriyama, M.; Ito, K.; Kato, T. *J. Am. Chem. Soc.* **2005**, *127*, 14769–14775.

(5) Schwab, A. D.; Smith, D. E.; Bond-Watts, B.; Johnston, D. E.; Hone, J.; Johnson, A. T.; de Paula, J. C.; Smith, W. F. *Nano Lett.* **2004**, *4*, 1261–1265.

tion. Cooperation and/or competition between the original $\pi-\pi$ interaction and additionally introduced intermolecular interaction lead to self-assembly of functional molecular materials into novel nanostructures with different morphology. As a consequence, incorporation of different functional groups onto the peripheral positions of conjugated molecules has been widely utilized to tune the morphology of self-assembled nanostructures. For example, cooperation between the $\pi-\pi$ interaction and hydrogen bonding among the molecules of phthalocyanine copper complexes decorated with optically active diol units was revealed to lead to the formation of fibrous assemblies.[22] Additional sulfur–sulfur interaction between the thioether side chains at the peripheral positions of phthalocyanine ring promotes the intermolecular $\pi-\pi$ interaction, which in turn induces the self-assembly of corresponding phthalocyanine molecules into rodlike aggregates.[23] Incorporation of different side chains onto different positions of the perylene diimide ring has been revealed to induce different effects on the intermolecular interactions, which in turn results in formation of nanostructures with different morphology according to Zang and

co-workers.[24,25] Very recently, this group incorporated different numbers of hydroxyl groups onto the meso-substituted phenyl groups of porphyrin ligand in mixed (phthalocyaninato)(porphyrinato) europium triple-decker complexes to tune the intermolecular interaction.[26] Cooperation and/or competition between the intermolecular $\pi-\pi$ interaction and hydrogen bonding for different sandwich mixed (phthalocyaninato)(porphyrinato) europium triple-decker compounds result in the formation of nanostructures with different morphologies. However, self-assembly of functional molecular materials into a prerequisite nanostructure with desirable dimension and morphology through controlling intermolecular interaction still remains a great challenge.

As the typical representative of functional molecular materials with large conjugated electronic molecular structure, porphyrins have been extensively studied over the past century because of their wide range of biological relevance and industrial applications.[27] In recent years, the self-assembly behavior and nanostructures of these tetrapyrrole derivatives have also started to attract extensive research interests. For example, hollow capsules with potential application as drug delivery agents were produced using a phase-transfer method depending on the strong $\pi-\pi$ interaction between porphyrin molecules.[28] Nanotubes with photocatalytic activity were synthesized by electrostatic force between two oppositely charged porphyrins.[29] Investigation over the organogel formation properties of a series of porphyrins with amide groups as peripheral hydrogen bonding sites indicates that the aggregation mode of porphyrin stacks can be tuned by the hydrogen-bonding interaction.[30] However, as mentioned above, great efforts have been continuously paid toward self-assembling porphyrin molecules into prerequisite nanostructures with desirable dimension and morphology by optimizing intermolecular interaction.

In the present article, we describe the design, synthesis, single crystal structure, and self-assembly properties of two novel 5,15-di[4-(5-acetylsulfanylpentyloxy)phenyl]porphyrin derivatives, namely $H_2[DP(CH_3COSC_5H_{10}O)_2P]$ (**1**) and $Zn[DP(CH_3COSC_5H_{10}O)_2P]$ (**2**) (Scheme 1). Introduction of the two carbonyl side chains onto the meso-attached phenyl groups in the tetrapyrrole ligand of porphyrin ring and in particular the central zinc ion induces additional metal–ligand coordination bonding interaction between neighboring molecules of porphyrinato zinc complex **2** in addition to intermolecular $\pi-\pi$ interaction, leading to the formation of nanostructures with different morphology in both MeOH and *n*-hexane in comparison with those of metal-free porphyrin **1** and clearly revealing the effect of coordination bonding interaction in tuning the intermolecular interaction between porphyrin molecules in the self-assembly process. This

(6) Wang, Z.; Li, Z.; Medforth, C. J.; Shelnutt, J. A. *J. Am. Chem. Soc.* **2007**, *129*, 2440–2441.

(7) (a) Yan, D. Y.; Zhou, Y. F.; Hou, J. *Science* **2004**, *303*, 65–67. (b) Shimizu, T.; Masuda, M.; Minamikawa, H. *Chem. Rev.* **2005**, *105*, 1401–1444. (c) Zhi, L.; Gorelik, T.; Wu, J.; Kolb, U.; Mullen, K. *J. Am. Chem. Soc.* **2005**, *127*, 12792–12793. (d) Hu, J.-S.; Guo, Y.-G.; Liang, H.-P.; Wan, L.-J.; Jiang, L. *J. Am. Chem. Soc.* **2005**, *127*, 17090–17095.

(8) (a) Shi, Z.; Li, Y.; Gong, H.; Liu, M.; Xiao, S.; Liu, H.; Li, H.; Xiao, S.; Zhu, D. *Org. Lett.* **2002**, *4*, 1179–1182. (b) Xiao, S.; Li, Y.; Fang, H.; Li, H.; Liu, H.; Shi, Z.; Jiang, L.; Zhu, D. *Org. Lett.* **2002**, *4*, 3063–3066. (c) Li, Y.; Wang, N.; Gan, H.; Liu, H.; Li, H.; Li, Y.; He, X.; Huang, C.; Cui, S.; Wang, S.; Zhu, D. *J. Org. Chem.* **2005**, *70*, 9686–9692. (d) Liu, Y.; Li, Y.; Jiang, L.; Gan, H.; Liu, H.; Li, Y.; Zhuang, J.; Lu, F.; Zhu, D. *J. Org. Chem.* **2004**, *69*, 9049–9054. (e) Gan, H.; Li, Y.; Liu, H.; Wang, S.; Li, C.; Yuan, M.; Liu, X.; Wang, C.; Jiang, L.; Zhu, D. *Biomacromolecules* **2007**, *8*, 1723–1729.

(9) Liu, R.; Holman, M. W.; Zang, L.; Adams, D. M. *J. Phys. Chem. A* **2003**, *107*, 6522–6526.

(10) Holman, M. W.; Liu, R.; Zang, L.; Yan, P.; DiBenedetto, S. A.; Bowers, R. D.; Adams, D. M. *J. Am. Chem. Soc.* **2004**, *126*, 16126–16133.

(11) Sauer, M. *Angew. Chem., Int. Ed.* **2003**, *42*, 1790–1793.

(12) Grimsdale, A. C.; Müllen, K. *Angew. Chem., Int. Ed.* **2005**, *44*, 5592–5629.

(13) (a) Xu, B. Q.; Xiao, X.; Yang, X.; Zang, L.; Tao, N. J. *J. Am. Chem. Soc.* **2005**, *127*, 2386–2387. (b) Guo, Y.; Li, Y.; Xu, J.; Liu, X.; Xu, J.; Lv, J.; Huang, C.; Zhu, M.; Cui, S.; Jiang, L.; Liu, H.; Wang, S. *J. Phys. Chem. C* **2008**, *112*, 8223–8228.

(14) Li, X.; Xu, B. Q.; Xiao, X.; Yang, X.; Zang, L.; Tao, N. J. *Faraday Discuss.* **2006**, *131*, 111–120.

(15) (a) Jiang, J.; Ng, D. K. P. *Acc. Chem. Res.* [Online early access]. DOI: 10.1021/ar800097s. Published Online: Sept 4, 2008. http://pubs.acs.org/cgi-bin/abstract.cgi/achre4/asap/abs/ar800097s.html. (b) Chen, Y.; Su, W.; Bai, M.; Jiang, J.; Li, X.; Liu, Y.; Wang, L.; Wang, S. *J. Am. Chem. Soc.* **2005**, *127*, 15700–15701. (c) Li, R.; Ma, P.; Dong, S.; Zhang, X.; Chen, Y.; Li, X.; Jiang, J. *Inorg. Chem.* **2007**, *46*, 11397–11404.

(16) Schmidt-Mende, L.; Fechtenkotter, A.; Mullen, K.; Moons, E.; Friend, R. H.; MacKenzie, J. D. *Science* **2001**, *293*, 1119–1122.

(17) Gregg, B. A. *J. Phys. Chem. B* **2003**, *107*, 4688–4698.

(18) Gregg, B. A. *J. Phys. Chem.* **1996**, *100*, 852–859.

(19) Tamizhmani, G.; Dodelet, J. P.; Cote, R.; Gravel, D. *Chem. Mater.* **1991**, *3*, 1046–1053.

(20) (a) Li, Y.; Xiao, S.; Li, H.; Li, Y.; Liu, H.; Lu, F.; Zhuang, J.; Zhu, D. *J. Phys. Chem. B* **2004**, *108*, 6256–6260. (b) Xiao, S.; Li, Y.; Li, Y.; Zhuang, J.; Wang, N.; Liu, H.; Ning, B.; Liu, Y.; Lu, F.; Fan, L.; Yang, C.; Li, Y.; Zhu, D. *J. Phys. Chem. B* **2004**, *108*, 16677–16685.

(21) Peeters, E.; Van Hal, P. A.; Meskers, S. C. J.; Janssen, R. A. J.; Meijer, E. W. *Chem.−Eur. J.* **2002**, *8*, 4470–4474.

(22) Kimura, M.; Muto, T.; Takimoto, H.; Wada, K.; Ohta, K.; Hanabusa, K.; Shirai, H.; Kobayash, N. *Langmuir* **2000**, *16*, 2078–2082.

(23) Minch, B. A.; Xia, W.; Donley, C. L.; Hernandez, R. M.; Carter, C.; Carducci, M. D.; Dawson, A.; O'Brien, D. F.; Armstrong, N. R. *Chem. Mater.* **2005**, *17*, 1618–1627.

(24) Balakrishnan, K.; Datar, A.; Naddo, T.; Huang, J.; Oitker, R.; Yen, M.; Zhao, J.; Zang, L. *J. Am. Chem. Soc.* **2006**, *128*, 7390–7398.

(25) Su, W.; Zhang, Y.; Zhao, C.; Li, X.; Jiang, J. *ChemPhysChem* **2007**, *8*, 1857–1862.

(26) Lu, G.; Chen, Y.; Zhang, Y.; Bao, M.; Bian, Y.; Li, X.; Jiang, J. *J. Am. Chem. Soc.* **2008**, *130*, 11623–11630.

(27) (a) *The Porphyrin Handbook*; Kadish, K. M., Smith, K. M., Guilard, R., Eds.; Academic Press: San Diego, CA, 2000; Vols. *1−10*, 2003; Vols. *11−20*. (b) Hamza, I. *ACS Chem. Biol.* **2006**, *1*, 627–629. (c) Lo, P.-C.; Chan, C. M. H.; Liu, J.-Y.; Fong, W.-P.; Ng, D. K. P. *J. Med. Chem.* **2007**, *50*, 2100–2107. (d) Vanyúr, R.; Héberger, K.; Jakus, J. *J. Chem. Inf. Comput. Sci.* **2003**, *43*, 1829–1836.

(28) Li, Y.; Li, X.; Li, Y; Liu, H.; Wang, S.; Gan, H.; Li, J.; Wang, N.; He, X.; Zhu, D. *Angew. Chem., Int. Ed.* **2006**, *45*, 3639–3643.

(29) Wang, Z.; Medforth, C. J.; Shelnutt, J. A. *J. Am. Chem. Soc.* **2004**, *126*, 15954–15955.

(30) Shirakawa, M.; Kawano, S.-i.; Fujita, N.; Sada, K.; Shinkai, S. *J. Org. Chem.* **2003**, *68*, 5037–5044.

**Scheme 1.** Synthesis of 5,15-Di[4-(5-acetylsulfanylpentyloxy)phenyl]porphyrin Derivatives H$_2$[DP(CH$_3$COSC$_5$H$_{10}$O)$_2$P] (**1**) and Zn[DP(CH$_3$COSC$_5$H$_{10}$O)$_2$P] (**2**)
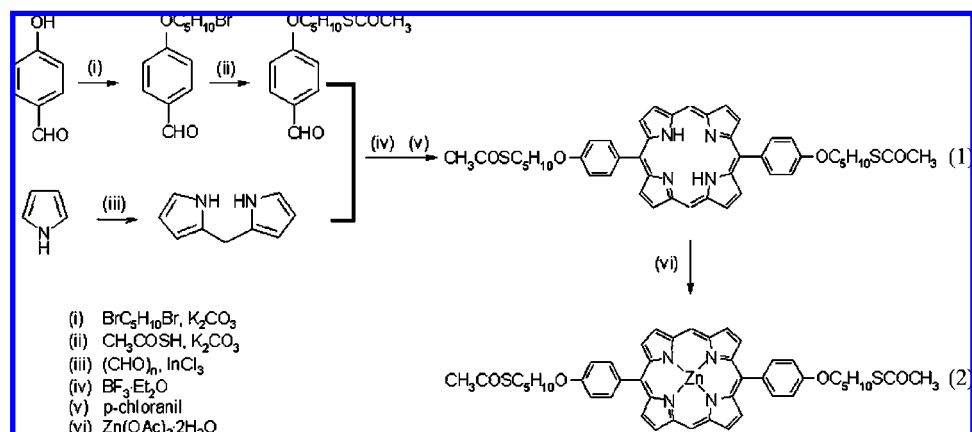


represents part of our continuous efforts toward understanding the relationship between the molecular structure and corresponding nanostructures of tetrapyrrole derivatives with large conjugated π system. Nevertheless, it is also worth noting that investigation of the formation mechanism of organic aggregates has stimulated great research interest associated with the important role toward preparing monodispersed organic nanostructures with controllable morphology and dimension for potential practical applications. However, because of the lack of single-crystal molecular structure for most organic frameworks used to construct organic nanostructures, the formation mechanism as well as the molecular packing conformation of corresponding self-assembled aggregates were usually proposed on the basis of aggregate X-ray diffraction (XRD) result (which is absent for a lot of cases) and the theoretical simulated molecular structure. This results in relatively high uncertainty in the proposed formation mechanism as well as proposed molecular packing conformation for organic self-assembled nanostructures. In the present work, the availability of single crystal and molecular structures revealed by XRD analysis for both porphyrin derivatives renders it possible to study the formation mechanism and molecular packing conformation of self-assembled nanostructures of these typical organic building blocks in a more confirmed manner.

## Results and Discussion

**Molecular Design, Synthesis, and Characterization.** Porphyrins are of typical large conjugated molecular electronic structure. The dominant intermolecular interaction among the porphyrin molecules is therefore π−π interaction. Tuning the intermolecular interaction of such a tetrapyrrole derivative can therefore be easily reached by incorporating functional groups (actually additional noncovalent interactions) onto the peripheral positions of porphyrin ring. On the basis of consideration of introducing additional metal−ligand coordination bonding interaction, two acetylsulfanylpentyloxy side chains were incorporated onto the meso-attached phenyl groups of diphenylporphyrin ring and zinc introduced into the center of the porphyrin ligand (Scheme 1).

The target metal-free porphyrin H$_2$[DP(CH$_3$COSC$_5$H$_{10}$O)$_2$P] (**1**) was synthesized in good yield from the reaction between thioacetic acid S-[5-(4-formylphenoxy)-pentyl] ester and dipyrromethane in the presence of BF$_3$·Et$_2$O in dichloromethane.[31,32] Its zinc complex Zn[DP(CH$_3$COSC$_5$H$_{10}$O)$_2$P] (**2**) was obtained from the reaction between metal-free porphyrin **1** and

Zn(OAc)$_2$·2H$_2$O in chloroform and methanol. Satisfactory elemental analysis results were obtained for both the two newly prepared porphyrin derivatives after repeated column chromatographic purification and recrystallization. The MALDI-TOF mass spectra of both compounds clearly showed intense signals for the molecular ion (M)$^+$/(HM)$^+$. The isotopic pattern closely resembles the simulated one as exemplified by the spectrum of compound **1** given in Figure S1 in the Supporting Information. These two new porphyrin compounds were also characterized with a range of spectroscopic methods. The $^1$H NMR spectra of compounds **1** and **2** were recorded in CDCl$_3$ at room temperature. All the signals can be readily assigned (Figure S2 and Table S1 in the Supporting Information).

**X-ray Single-Crystal Structures.** The crystal and molecular structures of porphyrin derivatives **1** and **2** were determined by XRD analyses. Single crystals of metal-free porphyrin **1** suitable for XRD analysis were obtained by slow diffusion of MeOH into the corresponding CHCl$_3$ solution. However, single crystals of porphyrianto zinc complex **2** were obtained from natural solvent evaporation of the chloroform solution of this compound in air. Compound **1** crystallizes in the monoclinic system with a P2(1)/c space group with two molecules in a unit cell. In contrast, compound **2** crystallizes in the triclinic system with a P1̄ space group with only one molecule per unit cell. It is worth noting that the crystal structure of the metal-free porphyrin contains four solvated CHCl$_3$ molecules. The crystal data are summarized in Table 1. Figure S3 in the Supporting Information shows the molecular structures of both metal-free porphyrin **1** and porhyrinato zinc complex **2** viewed along the $C_2$ axis, from which their tetrapyrrole nature and in particular molecular dimension are clearly revealed.

Figure 1 shows the crystal packing diagrams for both porphyrin derivatives. As revealed in the crystal-packing diagram of metal-free porphyrin **1** (Figure 1A), the solvated chloroform molecules connect neighboring metal-free porphyrin molecules into a face-to-face stacking supramolecular structure (H-aggregate) depending on the C−H···π interaction in the crystal of **1**, leading to a relatively large separation between the neighboring metal-free porphyrin rings, 5.19 Å. This in turn

(31) (a) Nagarkatti, J. P.; Ashley, K. R. *Synthesis* **1974**, 186–187. (b) Treibs, A.; Haberle, N. *Liebigs Ann. Chem.* **1968**, *718*, 183–191. (c) Wallace, D. M.; Leung, S. H.; Senge, M. O.; Smith, K. M. *J. Org. Chem.* **1993**, *58*, 7245–7257.

(32) Laha, J. K.; Dhanalekshmi, S.; Taniguchi, M.; Ambroise, A.; Lindsey, J. S. *Org. Process Res. Dev.* **2003**, *7*, 799–812.

**Table 1.** Crystallographic Data for Compounds **1** and **2**

|  | 1 | 2 |
|---|---|---|
| formula | $C_{46}H_{46}O_4N_4S_2 \cdot 2CHCl_3$ | $C_{46}H_{44}O_4N_4S_2Zn$ |
| $M_r$ | 1021.77 | 846.41 |
| crystal size (mm$^3$) | $0.21 \times 0.17 \times 0.15$ | $0.32 \times 0.23 \times 0.18$ |
| crystal system | monoclinic | triclinic |
| space group | $P21/c$ | $P\bar{1}$ |
| $a$ (Å) | 10.8849(3) | 10.6174(6) |
| $b$ (Å) | 22.7573(6) | 10.7550(8) |
| $c$ (Å) | 11.3839(3) | 11.2109(12) |
| $\alpha$ (deg) | 90.00 | 114.014(6) |
| $\beta$ (deg) | 116.2250(10) | 101.658(6) |
| $\gamma$ (deg) | 90.00 | 110.184(4) |
| $V$ (Å$^3$) | 2529.65(12) | 1006.18(14) |
| $Z$ | 2 | 1 |
| $F(000)$ | 1060 | 442 |
| $\rho_{calcd}$ (mg m$^{-3}$) | 1.341 | 1.397 |
| $\mu$ (mm$^{-1}$) | 0.468 | 0.764 |
| $\theta$ range (deg) | 2.09−25.00 | 2.17−25.05 |
| total no. of reflns | 21326 | 11732 |
| no. of independent reflns | 4409 ($R_{int} = 0.0320$) | 3460 ($R_{int} = 0.0588$) |
| parameters | 290 | 260 |
| R1 [$I > 2\sigma(I)$] | 0.0778 | 0.0743 |
| wR2 [$I > 2\sigma(I)$] | 0.2177 | 0.1965 |
| goodness of fit | 1.042 | 1.031 |

will result in a relatively weak $\pi-\pi$ interaction between neighboring stacking porphyrin ligands in the direction perpendicular to the porphyrin rings because of the relatively large intermolecular distance.

The porphyrinato zinc analogue **2** is packed differently in the crystal structure. As shown in Figure 1B, each porphyrinato zinc molecule is bound with two neighboring molecules, forming a head-to-tail porphyrin supramolecular chain (*J*-aggregate) via the Zn−O coordination bond between the central metal zinc of porphyrin molecule with the carbonyl oxygen in the aryloxy side chain of meso-attached phenyl groups in the neighboring porphyrin molecules. In the supramolecular chain of **2**, each Zn(II) metal ion complexed by four pyrrole nitrogen atoms of the porphyrin ligand is sandwiched between two pairs of antiparallel carbonyl arms of adjacent molecules because of the Zn−O coordination bonding, forming a slightly distorted octahedral geometry of zinc ion with the angle of Zn−O bond with respect to the N(pyrrole)$_4$ mean plane of porphyrin ring ranging from 84.48 to 95.52°. The distance between the coordinated oxygen and zinc is 2.60 Å, as expected, which is longer than that reported in pentacoordinated zinc porphyrin compound ZnTrTP (H$_2$TrTP = 5,10,15-triarylyl-20-quinone porphyrin), 2.28 Å.$^{33}$ The ring-to-ring separation of the two virtually parallel N(pyrrole)$_4$ mean planes of DP(CH$_3$COSC$_5$H$_{10}$O)$_2$P along the $C_2$ axis is 3.16 Å. This value is only a bit longer than that found in the bis(porphyrinato)thorium double-decker complex of Th(TPP)$_4$ reported earlier, 2.94 Å, in which the two porphyrin ligands are associated closely in a face-to-face manner by a thorium metal atom.$^{34}$ As a consequence, this result suggests feasible intense $\pi-\pi$ interaction between porphyrin rings along this $C_2$ axis direction. However, the separation between the two $C_2$ axes of neighboring Zn[DP(CH$_3$COSC$_5$H$_{10}$O)$_2$P] unit, 16.63 Å, is too far to induce effective $\pi-\pi$ interaction between porphyrin ligands in the direction perpendicular to the porphyrin ring (actually along the

$C_2$ axis direction). In contrast, $\pi-\pi$ interaction between neighboring porphyrin ligands in the direction along the supramolecular chain direction in the crystal of **2** is possible because of the close intermolecular distance in this direction. This is indeed demonstrated by the electronic absorption spectroscopic result of aggregates formed from this complex in both methanol and *n*-hexane as detailed below.

**Electronic Absorption Spectra.** The electronic absorption spectra of the two porphyrin derivatives **1** and **2** in CHCl$_3$ were recorded, and the data are compiled in Table 2. As expected, compound H$_2$[DP(CH$_3$COSC$_5$H$_{10}$O)$_2$P] (**1**) and Zn[DP(CH$_3$-COSC$_5$H$_{10}$O)$_2$P] (**2**) showed typical features of metal-free and zinc porphyrin compounds, respectively, in their electronic absorption spectra, revealing the nonaggregated molecular spectroscopic nature of both compounds in CHCl$_3$. As shown in Figure S4 in the Supporting Information, in line with that for H$_2$TPP (H$_2$TPP = 5,10,15,20-tetraphenylporphyrin),$^{35}$ the absorption around 410 nm for **1** can be attributed to the porphyrin Soret band, while the four typical weak absorptions at 504, 541, 578, and 633 nm can be attributed to the metal-free porphyrin Q bands. Upon complexation with zinc metal ion, the increase in the molecular symmetry from $C_{2h}$ for **1** to $D_{2h}$ for **2** induces change in the electronic absorption spectrum from typical feature for metal-free porphyrin to that for typical porphyrinato metal species (Figure S5 in the Supporting Information). With the porphyrin Soret band remaining unchanged at 410 nm, three weak Q absorptions appear at 501, 537, and 573 nm, respectively, for **2** in CHCl$_3$.

The aggregate electronic absorption spectra of these two porphyrin compounds in methanol and *n*-hexane are also recorded and given in Figures S4 and S5 in the Supporting Information, respectively, which are different from the spectra of corresponding compounds **1** and **2** in CHCl$_3$. Nevertheless, significant difference also exists in the electronic absorption spectrum between the two compounds in both methanol and *n*-hexane, indicating different aggregation type formed from metal-free porphyrin and porphyrinato zinc compounds in these two solvents. As shown in Figure S4 in the Supporting Information, the porphyrin Soret band at 410 nm in CHCl$_3$ for metal-free porphyrin **1** takes a slight blue shift to 404 and 406 nm, respectively, when dispersed in methanol and *n*-hexane, and the four porphyrin Q absorptions in chloroform also take a more or less blue shift (Table 2). However, introduction of zinc ion into the center of porphyrin ligand induces a significant red shift in all three porphyrin Q absorption bands for **2** from 501, 537, and 573 nm in CHCl$_3$ to 505, 544, and 581 nm in methanol and 508, 547, and 583 nm in *n*-hexane (Table 2) with the porphyrin Soret band remaining unchanged or slightly blue-shifted, respectively, indicating the effect of central zinc ion on the molecular packing conformation in aggregates due to the introduction of metal−ligand (Zn−O) coordination bonding. On the basis of Kasha's exciton theory,$^{36}$ blue shifts in the main absorption bands of the metal-free porphyrin **1** upon aggregation are typically a sign of the effective $\pi-\pi$ interaction between metal-free porphyrin molecules, indicating the formation of *H*-aggregate from the compound in both methanol and *n*-hexane. In contrast, the red-shifted absorption bands in the main electronic absorption spectra of porphyrinato zinc complex **2** upon aggregation in methanol and *n*-hexane imply the porphy-

(33) Senge, M. O.; Speck, M.; Wiehe, A.; Dieks, H.; Aguirre, S.; Kurreck, H. *Photochem. Photobiol.* **1999**, *70*, 206–216.

(34) Girolami, G. S.; Milam, S. N.; Suslick, K. S. *J. Am. Chem. Soc.* **1988**, *110*, 2011–2012.

(35) Ulman, A.; Manassen, J. *J. Am. Chem. Soc.* **1975**, *97*, 6540–6544.

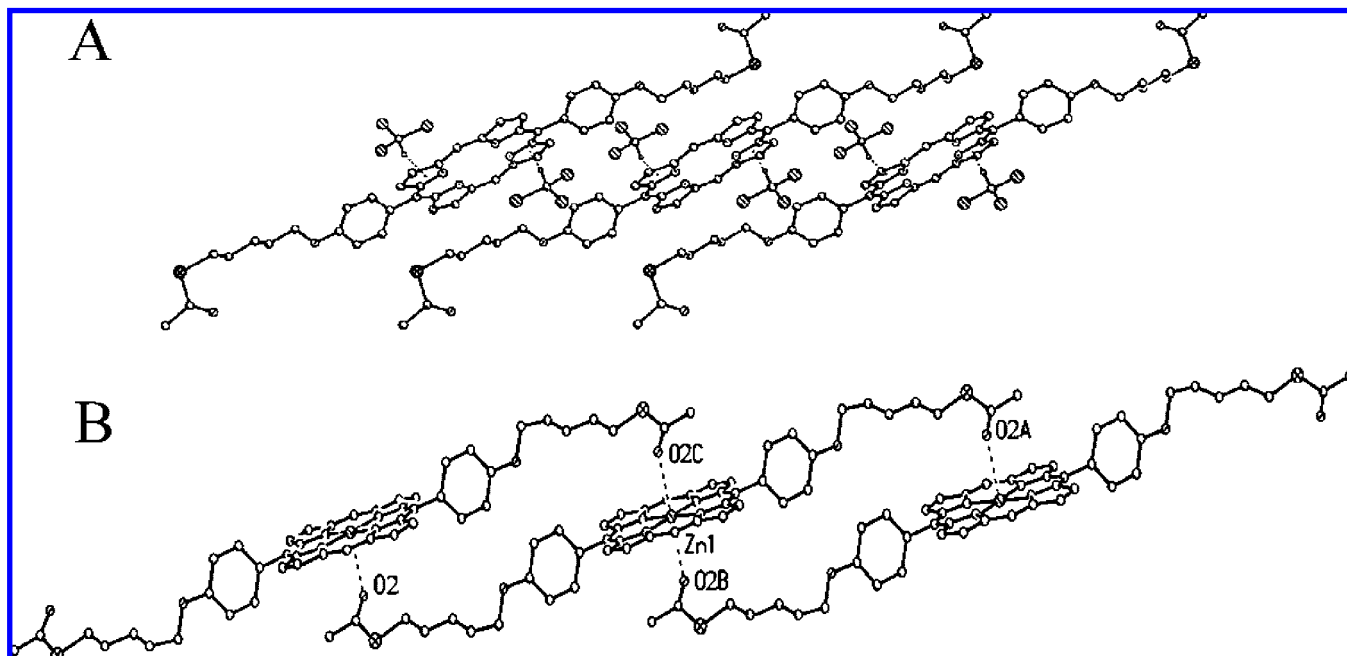(36) Kasha, M.; Rawls, H. R.; El-Bayoumi, M. A. *Pure Appl. Chem.* **1965**, *11*, 371–392.

**Figure 1.** Crystal-packing diagrams for $H_2[DP(CH_3COSC_5H_{10}O)_2P]$ (**1**) (A) and $Zn[DP(CH_3COSC_5H_{10}O)_2P]$ (**2**) (B) in side view. Hydrogen atoms are omitted for clarity.

***Table 2.*** Electronic Absorption Spectral Data for Compounds **1** and **2** Dissolved in $CHCl_3$ and the Self-Assemblies Dispersed in Methanol and *n*-Hexane

| compound | $\lambda$ (max/nm) | | |
|---|---|---|---|
| | $CHCl_3$ | methanol | *n*-hexane |
| **1** | 410, 504, 541, 578, 633 | 404, 501, 538, 576, 632 | 406, 501, 535, 578, 633 |
| **2** | 410, 501, 537, 573 | 410, 505, 544, 581 | 406, 508, 547, 583 |

rinato zinc molecules of this compound are enforced to adopt the *J*-aggregation mode. These results indicate the dominant role of $\pi-\pi$ interaction between the molecules of metal-free porphyrin **1** but of intermolecular metal–ligand coordination bonding due to the Zn–O coordination bond formed between central zinc ion of porphyrinato zinc molecule and a carbonyl oxygen atom in the aryloxy side chain of neighboring molecules for compound **2**, revealing the effect of metal–ligand coordination bonding interaction on tuning the intermolecular interaction of porphyrin molecules and in turn the aggregation mode. This is in good accordance with the single-crystal XRD analysis, XRD, and IR spectroscopic results as detailed above and below, respectively. In addition, comparison in the aggregate electronic absorption spectra for either metal-free porphyrin **1** or porphyrinato zinc complex **2** in methanol and *n*-hexane reveals the effect of the solvents on tuning the intermolecular interaction and in turn the molecular packing mode in aggregates due to different interaction between porphyrin and solvent molecules for both porphyrin derivatives.

**IR Spectra.** The IR spectra of these two porphyrin derivatives and their self-assembled nanostructures obtained are shown in Figures S6 and S7 in the Supporting Information. The similar feature in the IR spectra of the nanostructures to that of corresponding compounds for both $H_2[DP(CH_3COSC_5H_{10}O)_2P]$ (**1**) and $Zn[DP(CH_3COSC_5H_{10}O)_2P]$ (**2**) unambiguously confirms the composition of nanostructures from corresponding porphyrin compounds. In the IR spectrum of **1**, the absorption at 1684

$cm^{-1}$ is clearly due to the carbonyl vibration.[37] This is also true for the IR spectra of its aggregates formed in both methanol and *n*-hexane (Figure S6 in the Supporting Information). However, because of the formation of Zn–O coordination bond of the carbonyl oxygen in the aryloxy side chains in porphyrin molecule with zinc center of neighboring porphyrin molecule in the crystal of porphyrinato zinc analogue **2**, the typical carbonyl vibration splits into a shoulder band at 1688 and a main band at 1657 $cm^{-1}$ in the IR spectrum of **2** (Figure S7 in the Supporting Information), with the main absorption taking an obvious red shift in comparison with that for metal-free porphyrin **1**. As expected, split absorptions with the shoulder at 1691 or 1690 $cm^{-1}$ and main absorption at 1646 or 1661 $cm^{-1}$ were also observed in the IR spectrum of nanorods or hollow nanospheres formed from **2** in methanol or *n*-hexane (Figure S7 in the Supporting Information), indicating the formation of Zn–O coordination bond of the carbonyl oxygen in the aryloxy side chains in porphyrin molecule with zinc center of neighboring porphyrin molecules in these nanostructures.

**Morphology of the Aggregates.** The morphology of the aggregates formed was examined by scanning electron microscopy (SEM) and transmission electronic microscopy (TEM). Samples were prepared by casting a drop of sample solution onto a carbon-coated grid. The SEM images of aggregates of **1** and **2** were shown in Figure 2. It is well known that, according to the model set up by Srinivasarao and co-workers,[38] molecular materials dissolved in a solvent with density higher than that of water usually yield two-dimensional air bubbles and a three-dimensional network, respectively, after the natural evaporation of solvent in air in the cases of lack of and existence of significant intermolecular interaction. As shown in Figure 2A, a two-dimensionally ordered array of air bubbles with relatively high monodispersed pores with the diameter of ca. 500 nm was

(37) Orita, A.; Fukudome, M.; Ohe, K.; Murai, S. *J. Org. Chem.* **1994**, *59*, 477–481.
(38) Srinivasarao, M.; Collings, D.; Philips, A.; Patel, S. *Science* **2001**, *292*, 79–83.
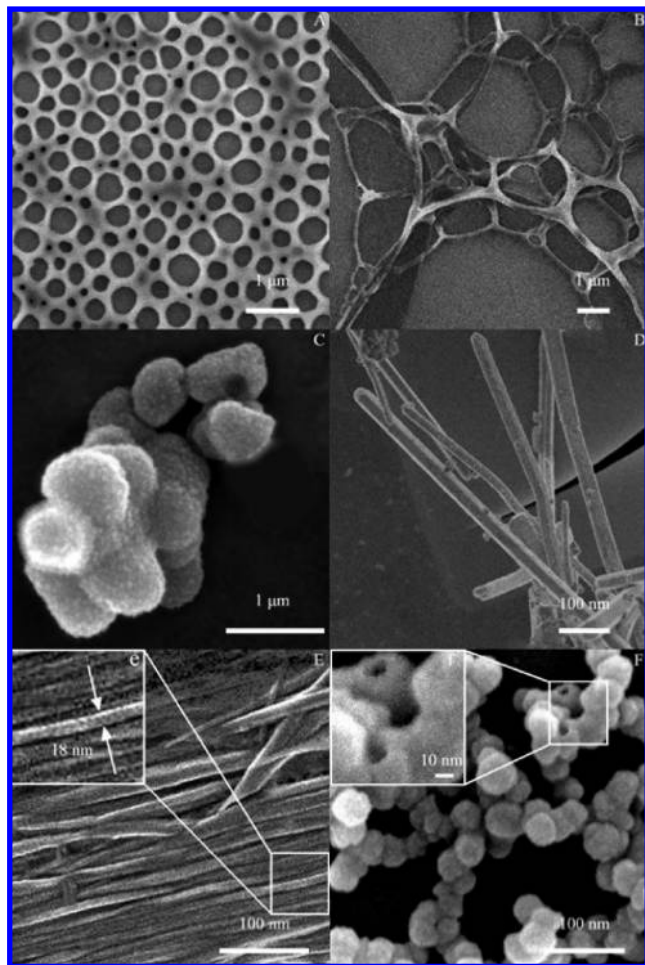
**Figure 2.** SEM images of nanostructures of compounds **1** and **2**. (A) Air bubbles formed from compound **1** in CHCl₃. (B) Three-dimensional network nanostructures formed from compound **2** in CHCl₃. (C) Nanoscale hollow spheres formed from compound **1** in methanol. (D) Nanorods formed from compound **2** in methanol. (E) Nanoribbons formed from compound **1** in *n*-hexane. (e) Zoom-in image of the rectangle part in E. (F) Nanoscale hollow spheres formed from compound **2** in *n*-hexane. (f) Zoom-in image of the rectangle part in F.

obtained by natural evaporation of the chloroform solution of metal-free porphyrin **1**,[38,39] indicating the less intermolecular interaction for this metal-free porphyrin compound **1** dissolved in chloroform. In good contrast, natural evaporation of the chloroform solution of porphyrianto zinc complex **2** led to the formation of three-dimensional network nanostructures (Figure 2B), revealing the significant intermolecular interaction due to the Zn–O coordination bond between the carbonyl oxygen in the aryloxy side chain of meso-attached phenyl group in porphyrin molecule with the zinc center of neighboring porphyrin molecules. This is in line with a previous result reported on another hexa-coordinated Zn(II) porphyrin complex, for which a three-dimensional coordination polymer was obtained through the same process.[40] When injecting a small volume of solution of these two compounds dissolved in CHCl₃ into methanol, different nanostructures were obtained. This is also

true for injecting a small volume of solution of these two compounds dissolved in CHCl₃ into *n*-hexane. Depending mainly on the intermolecular π–π interaction in cooperation with the van der Waals interaction, molecules of metal-free porphyrin **1** self-assemble into nanostructures with hollow sphere morphology with a diameter of ca. 700 nm (Figure 2C). The hollow interior nature is confirmed by the two broken spheres with hollow interior displayed at the top of Figure 2C. In the TEM image of Figure S8A in the Supporting Information, convincing hollow-sphere structures can be seen with the presence of circular rings of sectioned spheres and a cavity in the interior. As suggested by the single-crystal XRD analysis, Zn–O coordination bonding interaction between a carbonyl oxygen in the aryloxy side chain of meso-attached phenyl group in porphyrinato zinc molecule and the zinc center of neighboring molecules of **2** dominates the intermolecular interaction of the porphyrinato zinc compound. As a result, self-assembly of **2** induces the formation of nanostructures with nanorod morphology with ca. 50-nm width and 800-nm length (Figure 2D).

When the solvent is changed from methanol to *n*-hexane, further change in the morphology of self-assembled nanoscale aggregates was revealed, showing the solvent effect on the formation of self-assembled nanostructures. As can be seen from Figure 2E, molecules of metal-free porphyrin **1** self-assemble into nanostructures with nanoribbon morphology with uniform size and orientation. A zoom-in image of a piece of nanoribbon (Figure 2e) shows their average width of ca. 18 nm. The nanoribbons were ordered over several micrometers, in line with the long-range periodicity along the (010) direction as revealed by the XRD result due to the intermolecular π–π stacking interaction. For porphyrinato zinc complex **2**, self-assembly process in *n*-hexane leads to the formation of nanostructures with hollow sphere morphology with diameter of ca. 40 nm (Figure 2F). Figure 2f is a zoom-in image of some broken hollow spheres, revealing the hollow interior nature of nanospheres formed. Further evidence was given in Figure S8B in the Supporting Information, from which we can see that the inner compartments of the spheres are colorless.

At the end of this section, it is worth noting that, in line with the previous results of Hupp and co-workers,[41] the morphology of aggregates formed from the two porphyrin compounds **1** and **2** clearly shows dependence on the solvent it precipitated from since different solvent molecules with different mixing rates and viscosities can compete for specific intermolecular interaction moieties and therefore alter both the thermodynamics of the intermolecular interactions and the kinetics of the assembly process during nanomaterial formation.

**X-ray Diffraction Patterns of the Aggregates.** The nanostructures of the two compounds were fabricated by injecting a small volume of solution of **1** and **2** in chloroform (1 mM) into a large volume of methanol and *n*-hexane, respectively. The internal structure of self-assembled nanostructures of these two compounds was investigated by XRD analysis (Figures 3 and S9 in the Supporting Information). As shown in Figure 3A, in the low angle range, the XRD diagram of the nanoscale hollow spheres formed from compound **1** in methanol shows three refraction peaks at $2\theta = 1.76°$ (corresponding to 5.02 nm), 2.38° (3.71 nm), and 6.09° (1.45 nm), respectively, which are ascribed to the refractions from the (010), (100), and (001) planes.[23]

(39) (a) Schenning, A. P. H. J.; Benneker, F. B. G.; Geurts, H. P. M.; Liu, X. Y.; Nolte, R. J. M. *J. Am. Chem. Soc.* **1996**, *118*, 8549–8552. (b) Beysens, D.; Knobler, C. M. *Phys. Rev. Lett.* **1986**, *57*, 1433–1436. (c) Family, F.; Meakin, P. *Phys. Rev. Lett.* **1988**, *61*, 428–431. (d) Limaye, A. V.; Narhe, R. D.; Dhote, A. M.; Ogale, S. B. *Phys. Rev. Lett.* **1996**, *76*, 3762–3765.

(40) Teo, T.-L.; Vetrichelvan, M.; Lai, Y.-H. *Org. Lett.* **2003**, *5*, 4207–4210.

(41) Lee, S. J.; Hupp, J. T.; Nguyen, S. T. *J. Am. Chem. Soc.* **2008**, *130*, 9632–9633.
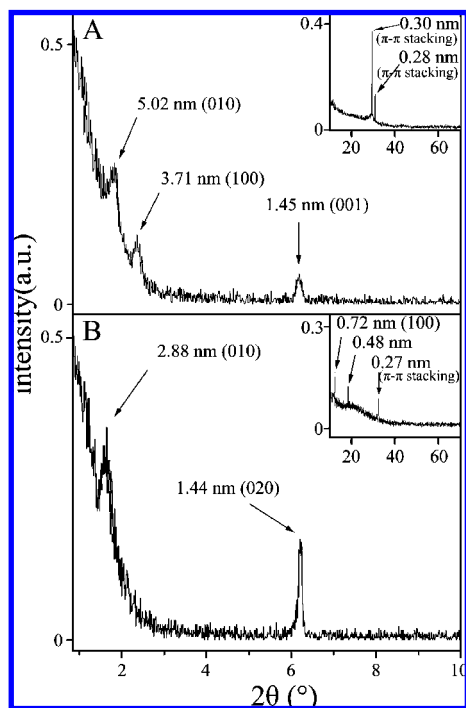
**Figure 3.** XRD profiles of the aggregates of compound **1** formed in methanol (A) and *n*-hexane (B).

These diffraction results could be assigned to the refractions from a parallelepipedal lattice (including monoclinic system) with cell parameters of $a = 3.71$, $b = 5.02$, and $c = 1.45$ nm (Figure 4). As can be seen from Figure S3A in the Supporting Information, the molecular dimensional size for **1** is 3.41 nm (length) × 1.06 nm (width) on the basis of single-crystal XRD analysis. According to the XRD result and the single-crystal molecular structure, the unit cell consisting of four molecules is given for metal-free porphyrin **1** (Figure 4B). Comparison between this unit cell of the nanoscale hollow spheres for **1** and that revealed for single crystals of the same compound formed also in methanol reveals their different molecular packing diagram, clearly indicating the effect of crystal growth speed on the system and dimension size of crystal unit cell. This is also true for the porphyrinato zinc complex as detailed below. It is worth noting that, in the wide-angle region, the XRD pattern presents two sharp refractions at $2\theta = 29.46$ and $30.96°$ (corresponding to 0.30 and 0.28 nm), respectively, which might be attributed to the distance between tetrapyrrole cores of neighboring stacking porphyrin molecules (Figure 4A). Because of the different experimental condition from the single crystals of the same compound, the solvent molecules of chloroform appear not to get into the aggregates, resulting in close intermolecular distance between neighboring stacking porphyrin molecules in the self-assembled nanostructures of **1** in comparison with that in single crystals.

As shown in Figure 3B, in the low-angle range, the XRD diagram of the nanoribbons formed from metal-free porphyrin compound **1** in *n*-hexane shows two narrow refraction peaks at 2.88 and 1.44 nm, which are ascribed to the refractions from the (010) and (020) planes, respectively. In addition, the XRD pattern also displays three well-defined peaks at 0.72, 0.48, and 0.27 nm. The former originates from the refraction of the (100) plane, whereas the latter two are assigned to the van der Waals distance between the pentyloxy side chains attached at the *meso*-phenyl groups of two neighboring porphyrin molecules and the

distance between tetrapyrrole cores of neighboring stacking porphyrin molecules, respectively. It is worth noting that the lack of the (001) refraction in the XRD diagram of the nanoribbons formed from metal-free porphyrin compound **1** in *n*-hexane indicates the lack of long-range periodicity along this direction in the self-assembled nanostructures of this metal-free porphyrin compound. As a result, growing in this direction during the self-assembly process is limited or prohibited. In contrast, observation of the higher-order refraction peak of the (010) plane suggests the advantage of crystal growth along this direction, resulting in the nanoribbons of the metal-free porphyrin.[42]

According to the XRD diffraction analysis result for the nanorods of porphyrinato zinc complex **2** formed in methanol (Figure S9A in the Supporting Information) and the single-crystal molecular structure size of this compound revealed by single-crystal XRD analysis (Figure S3B in the Supporting Information), the unit cell consisting of four porphyrinato zinc molecules from a parallelepipedal lattice (including triclinic system) with cell parameters of $a = 2.36$, $b = 8.74$, and $c = 0.91$ nm is given in Figure S10 in the Supporting Information for the nanorods of **2** formed in methanol. The sole sharp refraction at 0.31 nm for the nanorods of **2** formed in methanol in the wide-angle region can be assigned to the stacking distance between tetrapyrrole cores of neighboring porphyrin molecules (Figure S9 in the Supporting Information). This is in good accordance with that revealed by single-crystal X-ray analysis for this compound as detailed above. As revealed by the single-crystal XRD analysis of this compound, existence of the Zn−O coordination bond between the carbonyl oxygen in the aryloxy side chain of meso-attached phenyl group in porphyrinato zinc molecule with the zinc center of neighboring molecules of **2** induces the packing of porphyrinato zinc molecules in a one-dimensional direction. As a consequence, needlelike single crystals were obtained from this complex under suitable experimental condition in a macroscopic view. This is also responsible for the formation of aggregates with nanorod morphology during the self-assembly process of the same complex in methanol.[30]

The XRD pattern of self-assembled nanoscale hollow spheres of complex **2** in *n*-hexane shows two peaks at 5.56 and 4.96 nm in the low-angle region and six peaks at 0.63, 0.62, 0.52, 0.43, 0.31, and 0.26 nm in the wide-angle region (Figure S9B in the Supporting Information). As shown in Figure S11B in the Supporting Information, a unit cell consisting of two porphyrinato zinc molecules of **2** from a parallelepipedal lattice (including triclinic system) with cell parameters of $a = 4.96$, $b = 5.56$, and $c = 0.63$ nm can be concluded on the basis of this XRD result as well as the single-crystal molecular structure size of this compound. On the basis of the single-crystal XRD analysis result of **2**, the two diffraction peaks at 0.31 and 0.62 nm for the nanorods of **2** correspond to the stacking distance between porphyrin−porphyrin and porphyrin−porphyrin−porphyrin cores along the direction perpendicular to the porphyrin ring, respectively, whereas the two diffraction peaks at 0.26 and 0.52 nm correspond to the metal−ligand coordination bond length between zinc and oxygen and the two oxygen atoms coordinated with the central zinc atom below and above the porphyrin ring. The remaining peak at 0.43 nm is assigned to

(42) (a) Hudson, S. D.; Jung, H.-T.; Percec, V.; Cho, W.-D.; Johansson, G.; Ungar, G.; Balagurusamy, V. S. K. *Science* **1997**, *278*, 449–452. (b) Pan, Z. W.; Dai, Z. R.; Wang, Z. L. *Science* **2001**, *291*, 1947–1949.
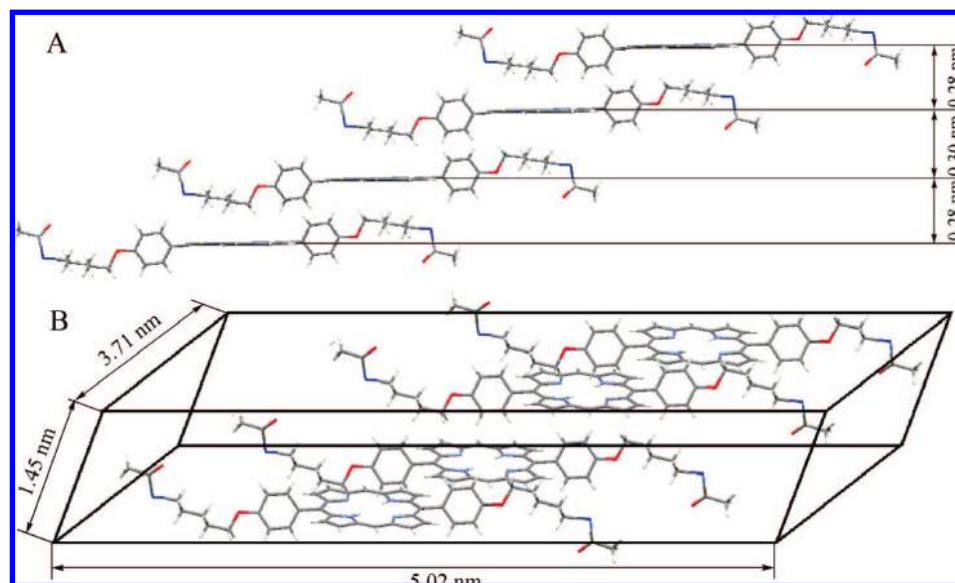
**Figure 4.** Schematic representation of the unit cell in the aggregates of compound **1** formed in methanol.

the van der Waals distance between the pentyloxy side chains attached at the *meso*-phenyl groups of two neighboring porphyrin molecules (Figure S9B in the Supporting Information).

At the end of this section, it is worth noting that the molecular packing as represented by the dimension of unit cell in the nanorods for **2** formed in methanol is different from that revealed for single crystals of the same complex formed also in methanol, which is also different from that calculated on the basis of experimental XRD data for the nanoscale hollow spheres of this complex formed in *n*-hexane. This is also true for the metal-free porphyrin **1**. These results are in good accordance with that for other tetrapyrrole derivatives as exemplified by 2,3,7,8,12, 13,17,18-tetracyclopentyl-5,10,15,20-*n*-pentylporphyrinato nickel complex and bis(phthalocyaninato)neodymium, for which different single crystals with different dimensions were obtained from different or even the same solvent,[43] confirming the effect of both solvent and growth speed on the system and size of crystal unit cell.

## Conclusions

In summary, we designed, synthesized, and investigated the self-assembly properties of two novel porphyrin derivatives with two 5-acetylsulfanylpentyloxy side chains at the opposite meso-attached phenyl groups. Comparative investigation results reveal that competition of intermolecular metal−ligand coordination bonding with the $\pi-\pi$ interaction between tetrapyrrole rings in tetrapyrrole molecules leads to different molecular packing conformation and in turn different self-assembled nanostructure morphology. The $\pi-\pi$ interaction dominates the formation of

nanostructures for metal-free porphyrin compound **1**, while the dominant Zn−O coordination bonding interaction between the carbonyl oxygen in the aryloxy side chain of meso-attached phenyl group in porphyrinato zinc molecule with the zinc center of neighboring molecules of **2** leads to nanostructures such as nanorods and hollow spheres for this complex in both methanol and *n*-hexane. In particular, availability of single crystal and molecular structure revealed by XRD analysis for both metal-free porphyrin and porphyrinato zinc compounds renders it possible to investigate the formation mechanism and the molecular packing conformation of self-assembled nanostructures for these typical organic building blocks with a large conjugated system in a more confirmed manner. The present result appears to represent the first effort toward realization of controlling and tuning the morphology of self-assembled nanostructures of porphyrin derivatives via molecular design and synthesis through the competition between intermolecular $\pi-\pi$ stacking interaction and metal−ligand coordination bonding interaction and, more importantly, is believed to be helpful toward preparation of monodispersed organic nanostructures with controllable morphology and dimension for potential practical applications.

## Experimental Section

**Measurements.** The nanostructures of the two compounds **1** and **2** were fabricated by the phase-transfer method according to the following procedure.[23,24,27,44,45] A minimum volume (30−50 μL) of concentrated chloroform solution of compounds (**1** and **2**) (1 mM) was injected rapidly into a large volume of methanol or *n*-hexane (1 mL), respectively, and subsequently mixed with a microinjector. The results were reproducible under the experimental

(43) (a) Medforth, C. J.; Senge, M. O.; Smith, K. M.; Sparks, L. D.; Shelnutt, J. A. *J. Am. Chem. Soc.* **1992**, *114*, 9859–9869. (b) Moskalev, P. N.; Shapkin, G. N.; Darovskikh, A. N. *Zh. Neorg. Khim.* **1979**, *24*, 340–346. (c) Darovskikh, A. N.; Tsishchenko, A. K.; Frank-Ka-menetskaya, O. V.; Fundamenskii, V. S.; Moskalev, P. N. *Kristal-lografiya* **1984**, *29*, 455–461. (d) Mossoyan-Deneux, M.; Pierrot, M.; Sorbier, J.-P.; Fournel, A.; Benlian, D. *C. R. Seances Acad. Sci., Ser. 2* **1986**, *303*, 669–672. (e) Darovskikh, A. N.; Frank-Kamenetskaya, O. V.; Fundamenskii, V. S. *Kristallografiya* **1986**, *31*, 901–905. (f) Darovsky, A.; Keserashvili, V.; Harlow, R.; Mutikainen, I. *Acta Crystallogr., Sect. B* **1994**, *50*, 582–588. Gong, X.; Milic, T.; Xu, C.; Batteas, J. D.; Drain, C. M. *J. Am. Chem. Soc.* **2002**, *124*, 14290–12491.

(44) SMART and SAINT for Windows NT Software Reference Manuals, version 5.0; Bruker Analytical X-Ray Systems: Madison, WI, 1997.

(45) (a) Kasai, H.; Nalwa, H. S.; Oikawa, H.; Okada, S.; Matsuda, H.; Minami, N.; Kakutal, A.; Ono, K.; Mukoh, A.; Nakanishi, H. *Jpn. J. Appl. Phys.* **1992**, *31*, 1132–1134. (b) Bertorelle, F.; Lavabre, D.; Fery-Forgues, S. *J. Am. Chem. Soc.* **2003**, *125*, 6244–6253. (c) Fu, H.; Xiao, D.; Yao, J.; Yang, G. *Angew. Chem., Int. Ed.* **2003**, *42*, 2883–2886. (d) Lee, S. J.; Jensen, R. A.; Malliakas, C. D.; Kanatzidis, M. G.; Hupp, J. T.; Nguyen, S. T. *J. Mater. Chem.* **2008**, *18*, 3640–3642. (e) Lee, S. J.; Malliakas, C. D.; Kanatzidis, M. G.; Hupp, J. T.; Nguyen, S. T. *Adv. Mater.* **2008**, *20*, 3543–3549.

conditions described above. ¹H NMR spectra were recorded on a Bruker DPX 300 spectrometer (300 MHz) in CDCl₃ using the residual solvent resonance of CHCl₃ at 7.26 ppm relative to that of SiMe₄ as internal reference. Electronic absorption spectra were recorded on a Hitachi U-4100 spectrophotometer. XRD experiment was carried out on a Rigaku D/max-γB X-ray diffractometer. MALDI-TOF mass spectra were taken on a Bruker BIFLEX III ultrahigh resolution Fourier transform ion cyclotron resonance mass spectrometer with α-cyano-4-hydroxycinnamic acid as matrix. Elemental analyses were performed by the Institute of Chemistry, Chinese Academy of Sciences. TEM images were measured on a JEOL-100CX II electron microscope operated at 100 kV. SEM images were obtained using a JEOL JSM-6700F field-emission scanning electron microscopy. For TEM imaging, a drop of sample solution was cast onto a carbon copper grid. For SEM imaging, gold (1−2 nm) was sputtered onto the grids to prevent charging effects and to improve the image clarity.

**Chemicals.** Column chromatography was carried out on silica gel (Merck, Kieselgel 60, 70−230 mesh) with the indicated eluents. All other reagents and solvents were used as received. The compound of dipyrromethane was prepared according to the published procedures.

**X-ray Crystallographic Analyses of 1 and 2.** Crystal data and details of data collection and structure refinement are given in Table 1. Data were collected on a Bruker SMART CCD diffractometer with an Mo Kα sealed tube ($\lambda = 0.71073$ Å) at 293 K, using a $\omega$ scan mode with an increment of 0.3°. Preliminary unit cell parameters were obtained from 45 frames. Final unit cell parameters were obtained by global refinements of reflections obtained from integration of all the frame data. The collected frames were integrated using the preliminary cell-orientation matrix. The SMART software was used for collecting frames of data, indexing reflections, and determining lattice constants, SAINT-PLUS was used for integration of intensity of reflections and scaling,[46] SADABS was used for absorption correction,[47] and SHELXL was used for space group and structure determination, refinements, graphics, and structure reporting.[46] CCDC-697437 and 697438 contain the supplementary crystallographic data for this article. These data can be obtained free of charge from the Cambridge Crystallographic Data Centre via www.ccdc.cam.ac.uk/data_request/cif.

(46) Sheldrick, G. M. SADABS, A Software for Empirical Absorption Correction; University of Göttingen: Göttingen, Germany, 1997.
(47) SHELXL Reference Manual, version 5.1; Bruker Analytical X-Ray Systems: Madison, WI, 1997.

**Supporting Information Available:** Preparation of 4-(5-bromopentyloxy)benzaldehyde; preparation of thioacetic acid *S*-[5-(4-formylphenoxy)pentyl]ester; preparation of metal-free 5,15-di[4-(5-acetylsulfanylpentyloxy)phenyl]porphyrin (**1**); preparation of 5,15-di[4-(5-acetylsulfanylpentyloxy)phenyl]porphyrinato zinc complex (**2**); experimental and simulated isotopic patterns for the molecular ion of the metal-free porphyrin (**1**); ¹H NMR spectra of H₂[DP(CH₃COSC₅H₁₀O)₂P] (**1**) and Zn[DP(CH₃-COSC₅H₁₀O)₂P] (**2**) in CDCl₃; molecular structures of metal-free **1** and porphyrinato zinc complex **2**; electronic absorption spectra of **1** and **2** in CHCl₃ and their self-assembled aggregates in methanol and *n*-hexane; IR spectra of compound **1**, aggregates of compound **1** with nanoscale hollow sphere morphology formed in methanol, and aggregates of compound **1** with nanoribbon morphology formed in *n*-hexane in the region 400−1800 cm⁻¹ with 2 cm⁻¹ resolution; IR spectra of compound **2**, aggregates of compound **2** with nanorod morphology formed in methanol, and aggregates of compound **2** with nanoscale hollow sphere morphology formed in *n*-hexane in the region 400−1800 cm⁻¹ with 2 cm⁻¹ resolution; TEM images of nanoscale hollow spheres formed from compounds **1** and **2** in methanol; XRD profiles of the aggregates of compound **1** formed in methanol and *n*-hexane; XRD profiles of the aggregates of compound **2** formed in methanol and *n*-hexane; schematic representation of the unit cell in the aggregates of compound **1** formed in methanol; schematic representation of the unit cell in the aggregates of compound **2** formed in methanol; schematic representation of the unit cell in the aggregates of compound **2** formed in *n*-hexane; and ¹H NMR spectroscopic data for the porphyrin derivatives **1** and **2**. This material is available free of charge via the Internet at http://pubs.acs.org.

JA8067337